3D Printed Cartilage-Like Tissue Constructs with Spatially Controlled Mechanical Properties

Bruna A. G. de Melo, Yasamin A. Jodat, Shreya Mehrotra, Michelle A. Calabrese, Tom Kamperman, Biman B. Mandal, Maria H. A. Santana, Eben Alsberg, Jeroen Leijten,* and Su Ryon Shin*

Developing biomimetic cartilaginous tissues that support locomotion while maintaining chondrogenic behavior is a major challenge in the tissue engineering field. Specifically, while locomotive forces demand tissues with strong mechanical properties, chondrogenesis requires a soft microenvironment. To address this challenge, 3D cartilage-like tissue is fabricated using two biomaterials with different mechanical properties: a hard biomaterial to reflect the macromechanical properties of native cartilage, and a soft biomaterial to create a chondrogenic microenvironment. To this end, a bath composed of an interpenetrating polymer network (IPN) of polyethylene glycol (PEG) and alginate hydrogel (MPa order compressive modulus) is developed as an extracellular matrix (ECM) with self-healing properties. Within this bath supplemented with thrombin, human mesenchymal stem cell (hMSC) spheroids embedded in fibrinogen are 3D bioprinted, creating a soft microenvironment composed of fibrin (kPa order compressive modulus) that simulate cartilage's pericellular matrix and allow a fast diffusion of nutrients. The bioprinted hMSC spheroids present high viability and chondrogenic-like behavior without adversely affecting the macromechanical properties of the tissue. Therefore, the ability to locally bioprint a soft and cell stimulating biomaterial inside of a mechanically robust hydrogel is demonstrated, thereby uncoupling the micro- and macromechanical properties of the 3D printed tissues such as cartilage.

1. Introduction

Articular cartilage has a limited capacity for self-repair, resulting in currently incurable degenerative joint diseases that affect millions of people around the world.[1] Consequently, the engineering of cartilage-like tissue constructs that possess chondrogenic and mechanical properties similar to those of native tissue represents a promising tool for effective cartilage repair. Numerous studies have attempted to engineer mechanically robust cartilage tissues by focusing on the development of novel biomaterials or scaffolds that would improve chondrogenic differentiation and cartilage formation.[2–5] During these processes, differentiated stem cells or chondrocyte cells deposit de novo formed extracellular matrices (ECMs) into the scaffolds, resulting in the realization of a stiffness that approximates that of native cartilage tissue. Although these approaches have successfully created cartilage-like tissue constructs, they take substantial amounts of time to reach their

Dr. B. A. G. de Melo, Dr. Y. A. Jodat, S. Mehrotra, Prof. S. R. Shin
Division of Engineering in Medicine
Department of Medicine
Harvard Medical School
Brigham and Women's Hospital
Cambridge, MA 02139, USA
E-mail: sshin4@bwh.harvard.edu

Dr. B. A. G. de Melo, Prof. M. H. A. Santana
Department of Engineering of Materials and Bioprocesses
School of Chemical Engineering
University of Campinas
Campinas, SP 13083-852, Brazil

Dr. Y. A. Jodat
Department of Mechanical Engineering
Stevens Institute of Technology
Hoboken, NJ 07030, USA

The ORCID identification number(s) for the author(s) of this article can be found under https://doi.org/10.1002/adfm.201906330.

S. Mehrotra, Dr B. B. Mandal
Department of Biosciences and Bioengineering
Indian Institute of Technology Guwahati
Guwahati, Assam-781039, India

Prof. M. A. Calabrese
Department of Chemical Engineering and Materials Science
University of Minnesota
Minneapolis, MN 55455, USA

Dr. T. Kamperman, Dr. J. Leijten
Department of Developmental BioEngineering
University of Twente
Enschede, Overijssel 7522 NB, The Netherlands
E-mail: jeroen.leijten@utwente.nl

Prof. E. Alsberg
Departments of Bioengineering and Orthopaedics
University of Illinois
Chicago, IL 60607, USA

desired mechanical properties. Moreover, the approaches' success vary heavily due to inter-donor variability. Alternatively, it is possible to engineer tissues that possess a cartilage-like stiffness upon creation, however, these materials are too stiff to support the cell's chondrogenic functions.[6] Therefore, achieving biomimicry of articular cartilage's load-bearing function in engineered equivalents has remained a challenge.

To overcome this challenge, we present a novel approach that emulates cartilage's mechanical properties by incorporating a spatially organized mechanical heterogeneity within the tissue's architecture. Specifically, natural cartilage's mechanical properties are derived from its hierarchical organization. For example, chondrocytes are located within a soft pericellular matrix (2–25 kPa) to maintain their chondrogenic phenotype, which, in turn, resides within a stiff ECM (0.5–4 MPa) to endow the tissue with its characteristic macromechanical tissue properties.[7–11] This natural hierarchical design was emulated in a deconstructed manner by creating a multimaterial tissue that was manufactured using embedded bioprinting. Specifically, a soft pericellular matrix (e.g., fibrin) containing chondrogenic cells was 3D bioprinted within a bath of mechanically robust ECM (e.g., PEG–alginate) in a spatially controlled manner. In this strategy, human bone marrow mesenchymal stem cells (hMSCs) were selected as the chondrogenic cell source, as they can be easily obtained from various different types of human tissues and allow for expansive and efficient cartilage matrix production, especially when formulated as limb bud emulating cellular microspheres.[12–15] We have previously demonstrated that, during construct maturation, encapsulated hMSC spheroids can autonomously disperse and form into a single cell tissue, as also occurs during the natural development from limb buds to mature cartilage.[13]

We report here that our alternative tissue design based on spatially organized bioprinting effectively endows engineered tissues with multiscale mechanical properties that reflect those found in natural cartilage, while allowing for chondrogenic behavior of hMSC microspheroids. Therefore, embedded 3D bioprinting technology can endow living constructs with near-paradoxical mechanical properties, e.g., being soft at the microlevel to stimulate encapsulated cells, yet being orders of magnitude stiffer at the macroscopic tissue level. It is anticipated that this innovative tissue engineering strategy based on natural and hierarchical designs will open up new opportunities to manufacture tissues with functionalities that rival those of healthy native tissues.

2. Results and Discussion

2.1. Design of Bioinks and Embedded Bioprinting System

To develop mechanically robust 3D cartilage-like tissue constructs, the crosslinked supporting bath should possess stiff and tough mechanical properties that are able to withstand high mechanical stresses and cyclic loads, while fibrin provides a soft and stimulating environment to cells. To this end, we first designed a hydrogel-based supporting bath possessing self-healing properties. This bath allowed successful printing of hMSC spheroid-laden bioink, without causing any permanent cracks, via an embedded bioprinting system (**Figure 1**). Cracks lead to the weakening of the supporting hydrogel as a whole via crack propagation under high mechanical cyclic loads; therefore, the self-healing process should occur rapidly (within a few seconds) around the printed bioink, ideally without using any added cytotoxic compounds or external stimuli to maintain high cell viability. To achieve these requirements, an interpenetrating polymer network (IPN) hydrogel composed of a light-induced covalently crosslinked dimethyl acrylate poly (ethylene glycol) (PEG) and a cation-induced physically crosslinked alginate prepolymer mixture was used as the self-healing supporting bath. These materials have the capability of mechanically
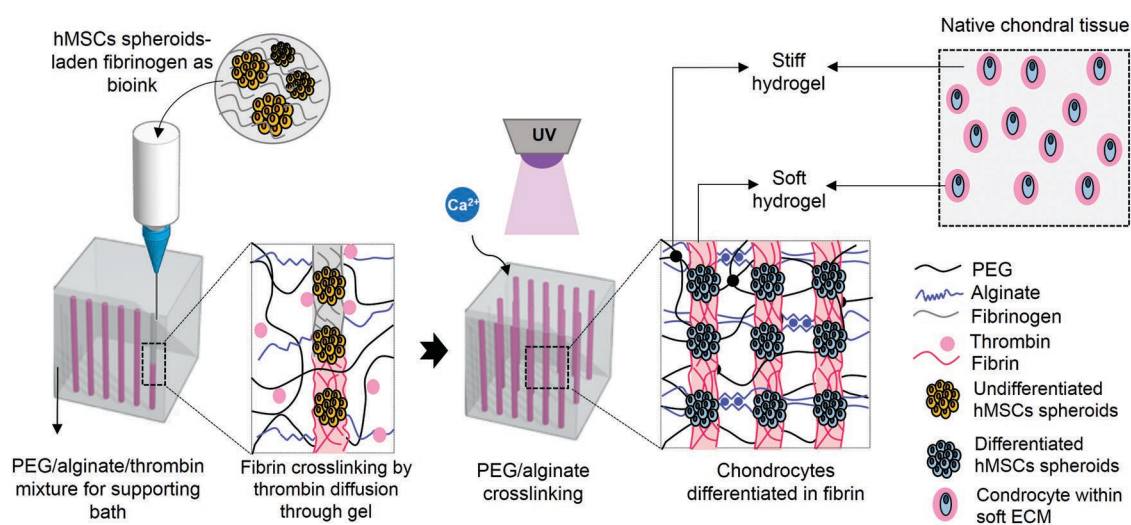

Figure 1. Schematic of the 3D bioprinting approach for the engineering of articular cartilage. hMSC-laden fibrinogen was used as a bioink for printing in a self-healing supporting bath of PEG–alginate prepolymer mixture, supplemented with thrombin. Thrombin interacted with fibrinogen and polymerized during bioprinting, forming soft fibrin fibers inside the hard PEG–alginate hydrogel and creating a suitable environment for chondrocyte differentiation within a mechanically robust construct. This system allows for the bioengineering of 3D native-like cartilage tissue.

**ADVANCED
SCIENCE NEWS**
www.advancedsciencenews.com

**ADVANCED
FUNCTIONAL
MATERIALS**
www.afm-journal.de

interlocking based on noncovalent (physical) supramolecular interactions between the two polymers, which is generally reversible.[16] In addition, the shear thinning behavior of the noncrosslinked alginate makes it a suitable candidate for one of the supporting bath materials.[17] After crosslinking, these biocompatible PEG–alginate polymer networks can possess high mechanical properties up to the MPa range, which is the same order of magnitude as native extracellular cartilage matrix, thus showing great potential for applications in cartilage repair.[16,18,19] Furthermore, these IPN hydrogels take up a large amount of water while maintaining their stiff, tough, and viscoelastic mechanical properties.[20] In a previous study, the PEG–alginate mixture was used as a bioink by Hong et al. to obtain a 3D cartilage tissue via extrusion-based bioprinting, and was shown to be a cytocompatible material, maintaining high cell viability for several days after printing.[16] Although the use of hard biomaterials as bioinks has proven to be suitable for cell growth, these materials may cause cellular stress associated with the hard mechanical microenvironments post gelation.[21] In addition, a direct interface with a stiff biomaterial is known to adversely affect cell survival and chondrogenic behavior after a few weeks of culture.[6] Importantly, they are also characterized by a poor diffusive capacity, which hinders the diffusion of nutrients and waste products through the hydrogel.

Therefore, to maintain chondrogenic function, a fibrin hydrogel was used as an appropriately soft biomaterial that is comparable to cartilage's pericellular matrix. In addition, it possesses a high diffusive capacity, which would overcome the diffusion limitation of the IPN hydrogels by allowing a fast permeation of nutrients, signaling molecules, and oxygen through the construct. This approach is expected to protect cells from undergoing apoptosis while stimulating their differentiation and maturation over time within the mechanically robust IPN hydrogel.[22,23] As previously reported, fibrin-based composite hydrogels have a strong capacity to maintain the phenotype of chondrocytes and promote synthesis of cartilage ECM.[24,25] The fibrin hydrogel network is formed following enzymatic polymerization of fibrinogen by thrombin.[26,27] However, as fibrin is a relatively viscous material, it will associate with poor cell viabilities when printing at high resolutions using small nozzles or high feeding speeds due to resulting high shear and extensional forces.[28,29] To solve this challenge, the hMSC spheroid-laden bioink utilized was fibrinogen. The mixture was printed in a PEG–alginate self-healing supporting bath containing thrombin, which diffused into printed fibrinogen to form a stable fibrin hydrogel. The diffusion based crosslinking process for the fibrin gel is ideal for locally depositing hMSC spheroid-laden soft matrices with high cell viability and high printing resolution due to fibrinogen's low viscosity and fast gelation.[30] After bioprinting and polymerization of the hMSC spheroid-laden fibrinogen bioink, the PEG–alginate prepolymer was dual-crosslinked to form an IPN hydrogel that possessed macromechanical properties similar to that of native cartilage, presenting high stiffness and toughness, which was assured by reversible physical crosslinks that allowed for energy dissipation, and covalent crosslinks that maintained hydrogel elasticity under deformation.[3,5,16]

2.2. Stiff and Viscoelastic PEG–Alginate IPN Hydrogel

Using a PEG and alginate prepolymer mixture, a multimaterial IPN hydrogel was fabricated through UV light and Ca^{2+}-mediated dual-crosslinking. The IPN's nature was characterized by a high stiffness due to the covalent crosslinking of PEG chains and a high toughness due to the alginate-Ca^{2+} crosslinking, which contributed to the dissipation of energy (**Figure 2**A). To optimize the polymer blend for use as a mechanically robust supporting hydrogel, PEG concentrations of 15, 20, and 25% were investigated, while the alginate concentration was fixed at 2.5%. This concentration was previously reported as being ideal for the fabrication of hydrogels with suitable toughness and biocompatibility for cartilage engineering.[16] Storage (G') and loss (G'') moduli analysis of the three hydrogel compositions demonstrated that the IPNs were predominantly elastic in nature as no G' variation was observed when varying the angular frequency from 1 to 100 rad s^{-1} (Figure 2B). PEG concentration directly influenced the hydrogel mechanical properties, with G' values around 0.15, 0.5, and 1 MPa for PEG 15, 20, and 25%, respectively. Additionally, the phase angle was close to zero for all PEG concentrations, confirming their solid-like behavior.[31] The maximum loss modulus was on the order of 10 kPa, indicating that more energy is stored in the hydrogels than is dissipated, which could cause cracks during compression to release energy.[31] However, no cracks were observed in the hydrogels, indicating that PEG chains were able to stabilize the deformation.[5,16] The compressive moduli were calculated from stress–strain curves, which showed a positive correlation with PEG concentration with values of 2.57 ± 0.04 MPa, 3.08 ± 0.09 MPa, and 4.43 ± 0.21 MPa for 15, 20, and 25% PEG-2.5% alginate, respectively (Figure 2C). These moduli demonstrate that PEG concentration positively correlates with material stiffness, in line with the existing literature.[7,32] As articular cartilage has a compressive modulus ranging from 0.08 to 2.5 MPa, the 15% PEG-2.5% alginate hydrogel possessed mechanical properties similar to native cartilage tissue.[10,33]

We also demonstrated the capacity of the PEG–alginate hydrogel to withstand mechanical loading by applying a cyclical strain of up to 40% compression to a 20% PEG-2.5% alginate IPN hydrogel. Hydrogels could return instantly to their original shape without cracking at 30% compressive strain and ≈1 MPa compressive stress (Figure 2D,F; Video S1, Supporting Information), which is in line with the mechanical behavior of native bovine cartilage.[10] The resilience capacity of the hydrogels was confirmed by their ability to recover their original shape after being loaded four times, and each time reaching larger values, with a maximum of 1.2, 1.7, and 2.4 MPa in the last cycle for PEG 15%, 20%, and 25%, respectively, indicating a PEG-concentration dependent effect on the materials' mechanical properties (Figure 2E–G). Moreover, the pronounced and stable hysteresis after five cycles confirmed the hydrogels' ability to dissipate energy when compressed,[3,4,34] which is assured by the reversible alginate-Ca^{2+} crosslinking (Figure 2H).

To assess the PEG–alginate IPN hydrogel's fluid phase, the swelling behavior of the PEG–alginate IPN hydrogel within phosphate buffered saline (PBS) was evaluated. PBS was used here in order to simulate the fluid phase present in the native articular cartilage tissue. After 8 h, the degree of swelling
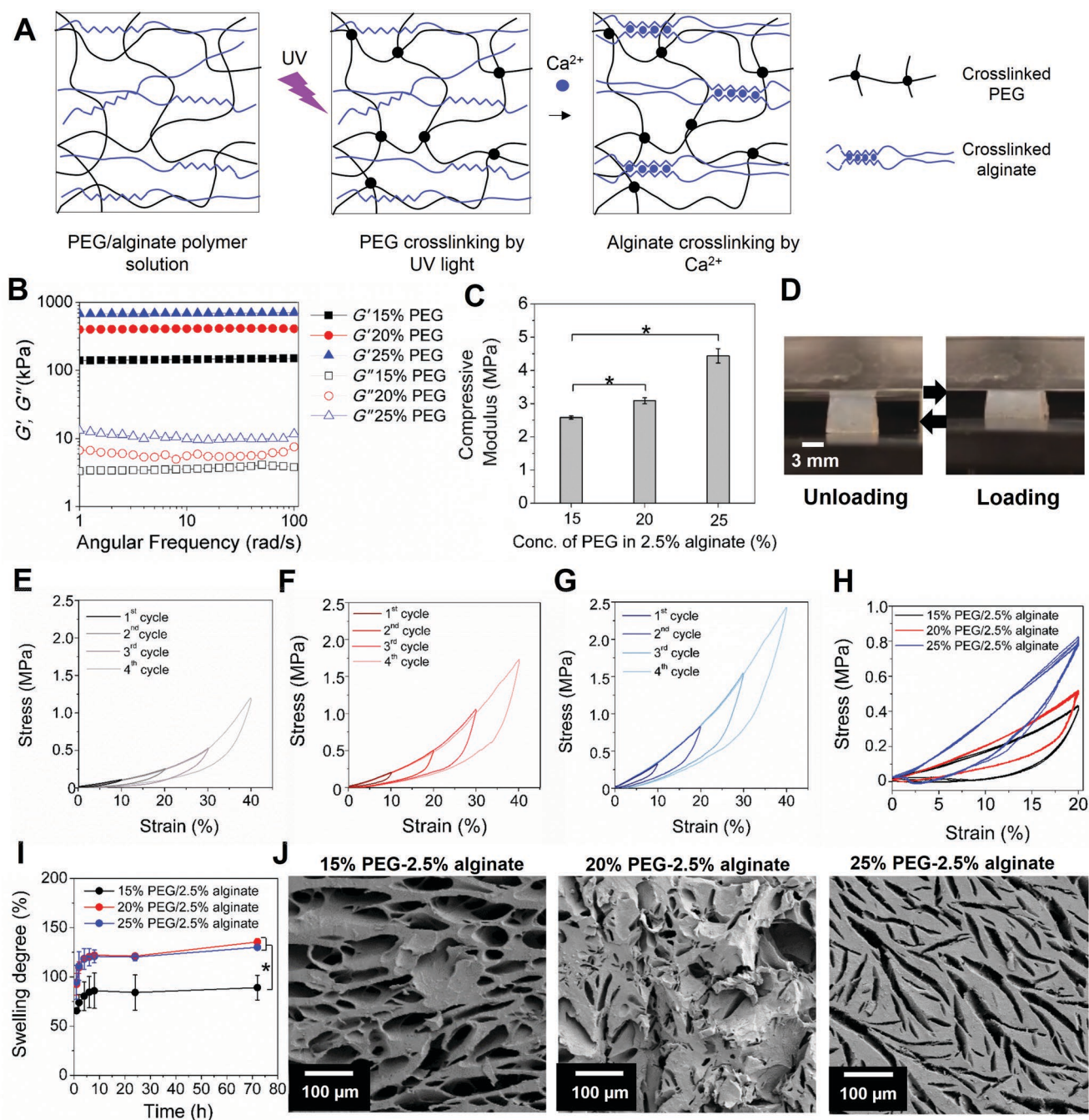
Figure 2. Characterization of PEG–alginate hydrogels with different PEG concentrations. A) Schematic illustration of the dual-crosslinking process to create the PEG–alginate IPN hydrogel. B) Linear rheological properties and C) compressive modulus of the PEG–alginate IPN hydrogels with various concentrations of PEG. *$p < 0.05$. D) Photographs of the 20% PEG–2.5% alginate IPN hydrogel under compressive strain at 30%. E–G) Cyclic compression test of the PEG–alginate IPN hydrogels with increased strain by a 10% increment with each compressive cycle from 10% to 40% for E) PEG 15%, F) PEG 20%, and G) PEG 25%. H) Cyclic compression test of the PEG–alginate IPN hydrogels with various concentrations of PEG under five repeated cycles of up to 20% strain. I) Swelling behavior of the PEG–alginate IPN hydrogels with various concentrations of PEG within PBS. *$p < 0.05$. J) SEM images showing the morphology of the 15%, 20%, and 25% PEG–2.5% alginate hydrogels.

reached equilibrium and no significant changes in time were observed, with a maximum swelling degree of 89.1 ± 12.6%, 135.5 ± 3.1%, and 130.3 ± 1.7% for PEG 15%, 20%, and 25%, respectively (Figure 2I). Consequently, the degree of swelling significantly increased by increasing PEG concentration from 15% to 20%. This was likely due to the increase of the hydrophilic

contents such as PEG in the IPN, resulting in a greater degree of binding of water molecules and a larger amount of water being contained in the networks. However, at 25% PEG, the degree of swelling plateaued, likely due to the IPN's crosslinking density countering the osmotic pressure of additional water molecules above 20% PEG.[35] As a result, the 15% PEG–alginate

IPN hydrogels contained similar amounts of water as native cartilage tissue, which is ≈80% of the wet weight of the tissue. Degradation of hydrogels composed of alginate can be accelerated in sodium citrate, which was previously found to improve cell proliferation.[36] Here, we observed that hydrogels presented a high level of stability, as mass loss was below 20% during the time studied, in which the 20% PEG–alginate IPN showed the lowest degradation rate in both PBS (control) and in sodium citrate solution (≈15% in 112 h) of the tested conditions (Figure S1A, Supporting Information). Specifically, mechanical properties of degraded hydrogels were assessed by evaluating the compressive modulus of IPNs incubated in the sodium citrate solution for 25 d. Results showed an approximately tenfold decrease in compressive modulus for 15% PEG–alginate hydrogel (0.24 ± 0.05 MPa), while higher concentrations of PEG conferred greater mechanical stability to the hydrogels, with an approximately fourfold compressive modulus decrease for 20% and 25% PEG–alginate hydrogels (0.78 ± 0.20 and 1.05 ± 0.17 MPa, respectively) (Figure S1B, Supporting Information). In line with this, scanning electron microscopy (SEM) images of freeze-dried PEG–alginate hydrogels potentially suggested that the hydrogels became progressively less porous and more dense when increasing the PEG concentration from 15% to 25% (Figure 2J). These results corroborated the formation of IPNs from the intra/intermolecular interactions, resulting in stiff hydrogels.[37] The high stiffness after degradation and capacity to withstand mechanical loading from cyclic strain suggested that our IPN hydrogels could have great potential for cartilage engineering and regeneration strategies.

2.3. Assessment of Bioprinting Conditions

In terms of compressive modulus, 15% PEG–2.5% alginate hydrogels performed similarly to native cartilage. However, we postulated that incorporation of the soft fibrin hydrogel within a bulk of stiff PEG–alginate hydrogels would result in a decrease in the overall mechanical properties of the hydrogel. Here, the 20% PEG–2.5% alginate composition was chosen for the supporting bath due to its stronger mechanical properties that might offset the expected reduced mechanical performance of the PEG–alginate hydrogel. Fibrinogen is a bioink with low viscosity and Newtonian behavior (Figures 3A and S2A, Supporting Information) that is difficult to bioprint via conventional extrusion-based bioprinting techniques without using thrombin to create stable microprinted lines.[38] This limitation was overcome by using the embedded bioprinting technique with the PEG–alginate supporting bath, which displayed a non-Newtonian, shear thinning (pseudoplastic) behavior (Figure S2B,C, Supporting Information). Prepolymers with increased concentrations of PEG (20% and 25%) presented an increased flow consistency index (K) and a decreased power law index (n) compared to that with 15% of PEG, showing that higher concentrations of PEG led to increased shear thinning (Table S1, Supporting Information). Shear thinning is an ideal flow characteristic for support baths to provide low mechanical resistance to the nozzle when bioprinting in an otherwise viscous bath. Moreover, pseudoplastic fluids behave as a rigid

body at low shear stresses, making it possible to sustain the shape and location of the printed microstructure (**Figure 3**A).[29] The presence of thrombin increased the zero-shear viscosity of the PEG–alginate prepolymer solution, which was 20.5 ± 6.4 Pa s as compared to the bath without the enzyme (11.7 ± 1.9 Pa s). This viscosity increase is likely due to the thrombin induced non-covalent supramolecular interactions, such as the ionic interaction between negatively charged carboxylate groups of sodium alginate and positively charged thrombin.[39] As expected, the fibrin zero-shear viscosity was substantially higher than that of fibrinogen, 16.9 ± 3.3 versus 3.9 ± 0.8 Pa s, respectively (Figure 3B).

The polymerization of fibrin gel is associated with increased turbidity (Figure 3C). The storage modulus of fibrin was significantly lower than that of the PEG–alginate hydrogels at equivalent frequencies, as was expected, reaching a maximum of 10 Pa (Figure 3D). The fibrin gel behaved distinctly from the tough hydrogels, showing a more prominent viscous behavior with increasing frequency, indicating its low capacity to store energy at higher frequencies. Mechanical analysis of fibrin showed low fracture stress (6.4 kPa) (Figure 3E), and a much lower compressive modulus than the PEG–alginate hydrogels (2.4 ± 0.8 kPa) at the same strain rate (10% to 20%), confirming the material's softness. It is anticipated that a fibrin hydrogel could therefore provide a softer microenvironment to encapsulated cells, which is expected to reduce the physical constraints compared to the dense and hard PEG–alginate IPN hydrogel for the hMSC spheroids. Moreover, fibrin hydrogels possessed a high permeability,[40] which could also further improve hMSC spheroids' viability within the PEG–alginate IPN hydrogel.

To locally combine the fibrin microhydrogel within a bulk of hard PEG–alginate IPN hydrogel, vertically oriented fibers were printed to control the arranged direction of chondrocytes, partially reproducing the overall native cartilage organization.[41] Bioprinting was characterized by testing the influence of the nozzle speed and bioink flow rate on the diameter of printed fibers. A needle with a 500 μm inner diameter was used for extrusion, and bioprinting was performed by varying bioink flow rates from 5 to 10 μL min^{-1} and nozzle speed from 50 to 600 mm min^{-1}. After printing, the PEG–alginate supporting bath was subsequently dual-crosslinked using UV light and 0.1 mol L^{-1} CaCl$_2$. By printing a fibrinogen bioink containing pink stain, it was optically verified that the printed lines possessed diameters between ≈50 to 250 μm, which was tightly controlled by the printing parameters bioink flow rate and nozzle speed (Figure 3F,G, Figure S3 and Video S2, Supporting Information). The minimum diameter of the printed lines was ≈50 μm, which is difficult to achieve via conventional extrusion-based printing. The bioprinted constructs presented a very precise alignment and high resolution deposition of fibrin, with width consistency along the construct length (Figure 3H-i–iii). Furthermore, the printing nozzle could continuously move up and down in the supporting bath without crack formation. Finally, the 3D printing created a complex-structured, multimaterial composite composed of a high resolution array of parallel lines within a distinct material bulk (Figure 3H-iv,v).

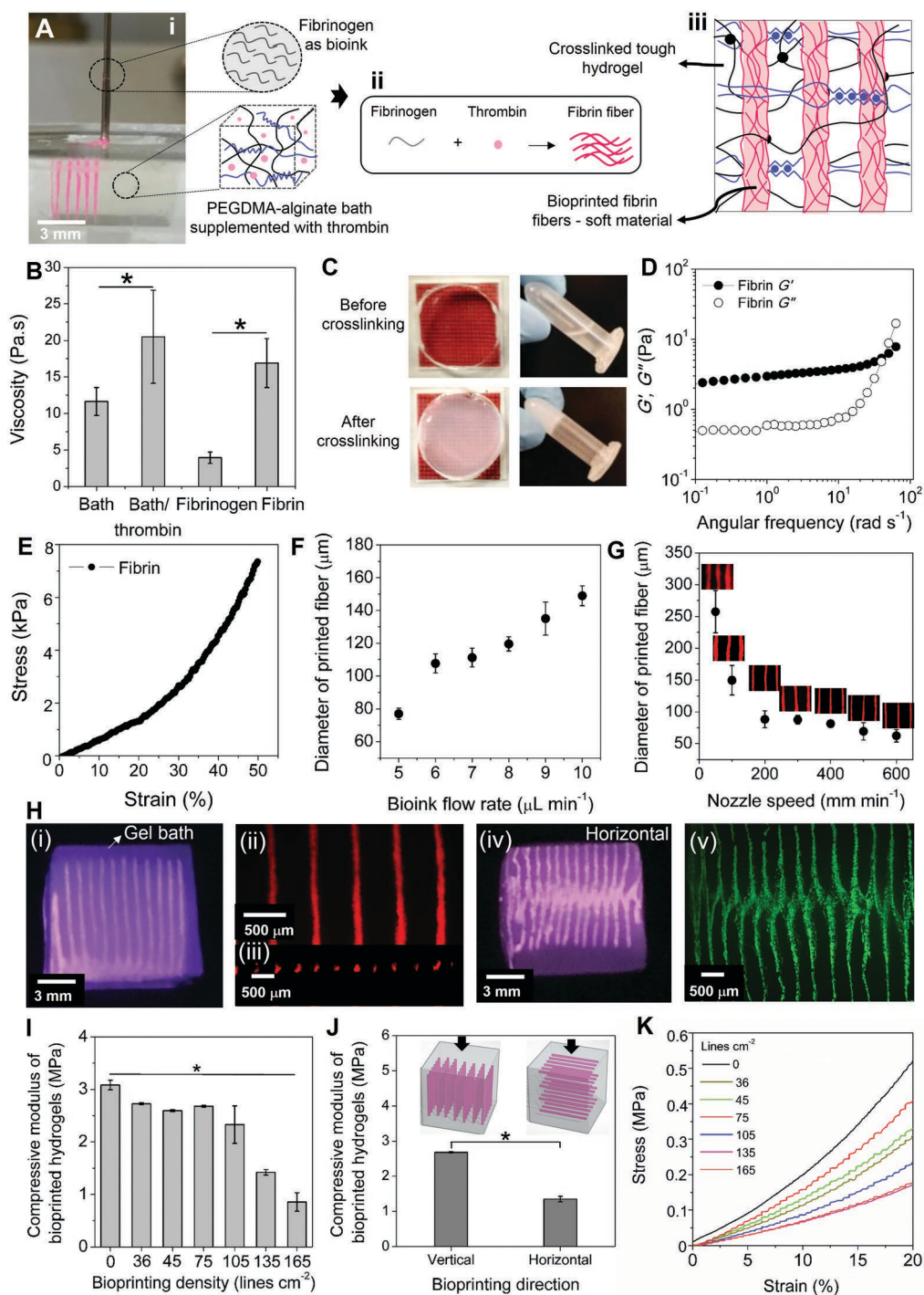To evaluate the effects of the internal soft fibrin hydrogel patterns on the overall mechanical properties of the

Figure 3. Characterization of the bioink and bioprinting conditions. A) Schematic of the 3D printing approach. i) Printing using fibrinogen solution as bioink stained pink, and PEG–alginate supplemented with thrombin as bath. ii) Schematic of the polymerization reaction between fibrinogen and thrombin forming fibrin. iii) Schematic of the fibrin printed lines in PEG–alginate bath, after crosslinking. B) Viscosity of the supporting bath (20% PEG–2.5% alginate) in the presence and absence of thrombin, and of the bioink before (fibrinogen) and after (fibrin) crosslinking. $*p < 0.05$. C) Images of bioink taken before and after crosslinking. D) Rheological properties and E) stress–strain curve of fibrin gel. F) Diameter of printed fibrin fibers as a function of bioink flow rate. G) Diameter of printed fibrin fibers with respect to nozzle speed. H) Images of bioprinted fibrin in 20% PEG–2.5% alginate. i) Photograph of vertically printed fibrin. Optical images of vertically printed fibrin from ii) side and iii) top views. iv) Photomicrograph of horizontally printed fibrin and v) optical image of horizontally printed fibrin from top view. I) Compressive modulus of IPN hydrogels containing different densities of printed lines in 20% PEG–2.5% alginate hydrogels. $*p < 0.05$. J) Compressive modulus of IPN hydrogels with bioprinted lines (105 lines cm^{-2}) in vertical and horizontal orientations in 20% PEG–2.5% alginate hydrogels. $*p < 0.05$. K) Stress–strain curves of PEG–alginate hydrogels with printed lines at different densities. $*p < 0.05$, $n = 3$.

PEG–alginate IPN hydrogel, the fibrinogen bioink was printed with various densities (36, 45, 75, 105, 135, and 165 lines cm^{-2}), as well as different orientations (Figure 3I–K, Figure S4, Supporting Information). Results show that up to 105 lines cm^{-2}, no major difference in the compressive modulus relative to the bulk PEG–alginate hydrogel (0 line cm^{-2}) was observed, with a loss in mechanical properties of ≈20%. Compressive modulus decreased for 135 lines cm^{-2} and 165 lines cm^{-2}, being 1.42 ± 0.05 and 0.86 ± 0.17 MPa, respectively, with a loss of compressive modulus higher than 50%, as compared to the bulk hydrogel, demonstrating that printing density adversely affected the macromechanical properties of the IPN hydrogel when exceeding a threshold value (Figure 3I). However, we hypothesize that the bioprinted hMSC spheroids-laden fibrin cultured within the PEG–alginate hydrogel might improve the mechanical stiffness of the surrounded soft fibrin and the overall construct after long-term culture, e.g., via ECM deposition.

We have also demonstrated that the printed line orientation could endow the engineered constructs with an anisotropic mechanical behavior that is characteristic for natural cartilage (Figure 3J). It is of note that, especially for low density printed constructs, a strain-stiffening behavior was observed, which may be interesting for the engineering of cartilage tissues that self-protect against trauma or rapid-loading induced rupture (Figure 3K).[42]

2.4. hMSC Spheroids Fabrication and Survival in Soft and Stiff Hydrogels

A polydimethylsiloxane (PDMS) microwell technique was used to form hMSC spheroids in high throughput (**Figure 4**A).[43] The PDMS mold was composed of 576 microwells with 200 µm height × 200 µm diameter (Figure 4B,C). Micrometer sized hMSC spheroids self-assembled over the course of 24 h when seeded in the microwells due to the significantly higher cell–cell interactions as compared to cell–substrate interactions.[44] In addition, the poor cell–substrate interaction properties of the PDMS microwell allowed for facile harvesting of the intact spheroids after 1 d of culture (Figure 4D,E). The harvested hMSC spheroids were characterized as having a narrow size distribution with diameters of 110 ± 22 µm (Figure 4F). This equated to ≈1700 cells per spheroid, which correlated with the expected number of cells based on seeding density. Live/dead analysis confirmed that hMSC spheroids remained viable after harvesting (Figure 4G).

To evaluate cell viability in the soft and hard hydrogels, hMSC spheroids were encapsulated and cultured for 7 d in bulk fibrin, bulk PEG–alginate, and fibrin that was homogeneously mixed into PEG–alginate (fibrin/PEG–alginate). The hMSC spheroids within the PEG–alginate and fibrin/PEG–alginate hydrogels had become smaller (diameter of 91.2 ± 15.9 and 93.6 ± 6.7 µm, respectively) than hMSC spheroids embedded in fibrin (140.6 ± 8.6 µm) (Figure 4H,J–L), and presented a less rounded shape (Figure 4I), which we hypothesize to be due to the physical constraints generated by the dense and high mechanical properties of the PEG–alginate hydrogel. Live/dead results revealed that there was an increase in the

viability of hMSC spheroids in the soft fibrin gel (Figure 4J–L, Figure S5A, Supporting Information), while the viability of hMSC spheroids decreased in the hard PEG–alginate IPN and in the mixed fibrin/PEG–alginate. On the seventh day, viability of hMSC spheroids in fibrin was 94.3 ± 0.4%, and in PEG–alginate and fibrin/PEG–alginate was 77.6 ± 3.1% and 77.7 ± 0.4%, respectively, which proved that fibrin gel is an excellent matrix to promote cell viability (Figure 4M).[22,45,46] Importantly, endowing hard PEG–alginate hydrogels homogeneously with fibrin did not improve spheroid viability, indicating the essential nature of spatial separation between the soft fibrin and the hard PEG–alginate hydrogel to allow for improved construct performance.

2.5. Mechanically Robust 3D Printed hMSC Spheroid-Laden Cartilage-Like Tissue Constructs

Vertically aligned fibrin lines were bioprinted, allowing for an organized deposition of spheroids inside the PEG–alginate IPN hydrogel (**Figure 5**A). SEM analysis confirmed the incorporation of hMSC spheroids within the fiber networks of the printed fibrin hydrogel (Figure 5B). The bioprinted hMSC spheroid-laden fibrin in the PEG–alginate IPN hydrogel showed good viability in both the core and the shell after 3, 5, and 7 d (Figure 5C). In addition, the hMSC spheroid-laden fibrin showed higher viability (91.2 ± 1.0%) on day 5 compared to hMSC spheroids that were directly encapsulated in a PEG–alginate IPN hydrogel without the printed fibrin gel (79.3 ± 1.8%) (Figure 5D). The bioprinted hMSC spheroids that had their own soft pericellular matrix with the fibrin gel showed high viability compared with that of the simply mixed fibrin/PEG–alginate hydrogels (Figure 4M). The metabolic activity of hMSC spheroids within fibrin fibers that were printed in the PEG–alginate IPN hydrogel was significantly greater than that of spheroids cultured directly in the PEG–alginate hydrogel by day 3 and this increase was maintained over 7 d (Figure 5E). Furthermore, bioprinted spheroids did not form a necrotic core in 21 d of incubation, showing a low number of apoptotic cells (Figure S6, Supporting Information). This indicates that soft fibrin gel could facilitate enhanced nutrient and oxygen diffusion through the hard hydrogel, resulting in higher viability and growth of spheroids and even induced cell spreading into the soft matrix.[47]

In order to corroborate this hypothesis, the diffusive properties of fibrin and PEG–alginate hydrogels were evaluated using fluorescein isothiocyanate (FITC) labeled dextran. PEG–alginate IPN showed permeability below 10% for dextran-FITC larger than 3.3 nm of hydrodynamic radius (20 kDa), while molecules of an increased radius (6 nm, 70 kDa) could more easily permeate soft fibrin hydrogels (Figure 5F). Time-lapse confocal imaging revealed a significant decrease in the fluorescence intensity of 20 kDa dextran-FITC permeated in PEG–alginate IPN as compared to fibrin, in which after 18 h, loss of fluorescence signal was ≈80% and ≈30% in the deepest layer of PEG–alginate and fibrin hydrogels, respectively (Figure 5G,H). Moreover, dextran–FITC diffusion in PEG–alginate was about tenfold slower than in fibrin (Figure 5I), which showed a diffusive coefficient, D, of 24 ± 1 µm^2 s^{-1}
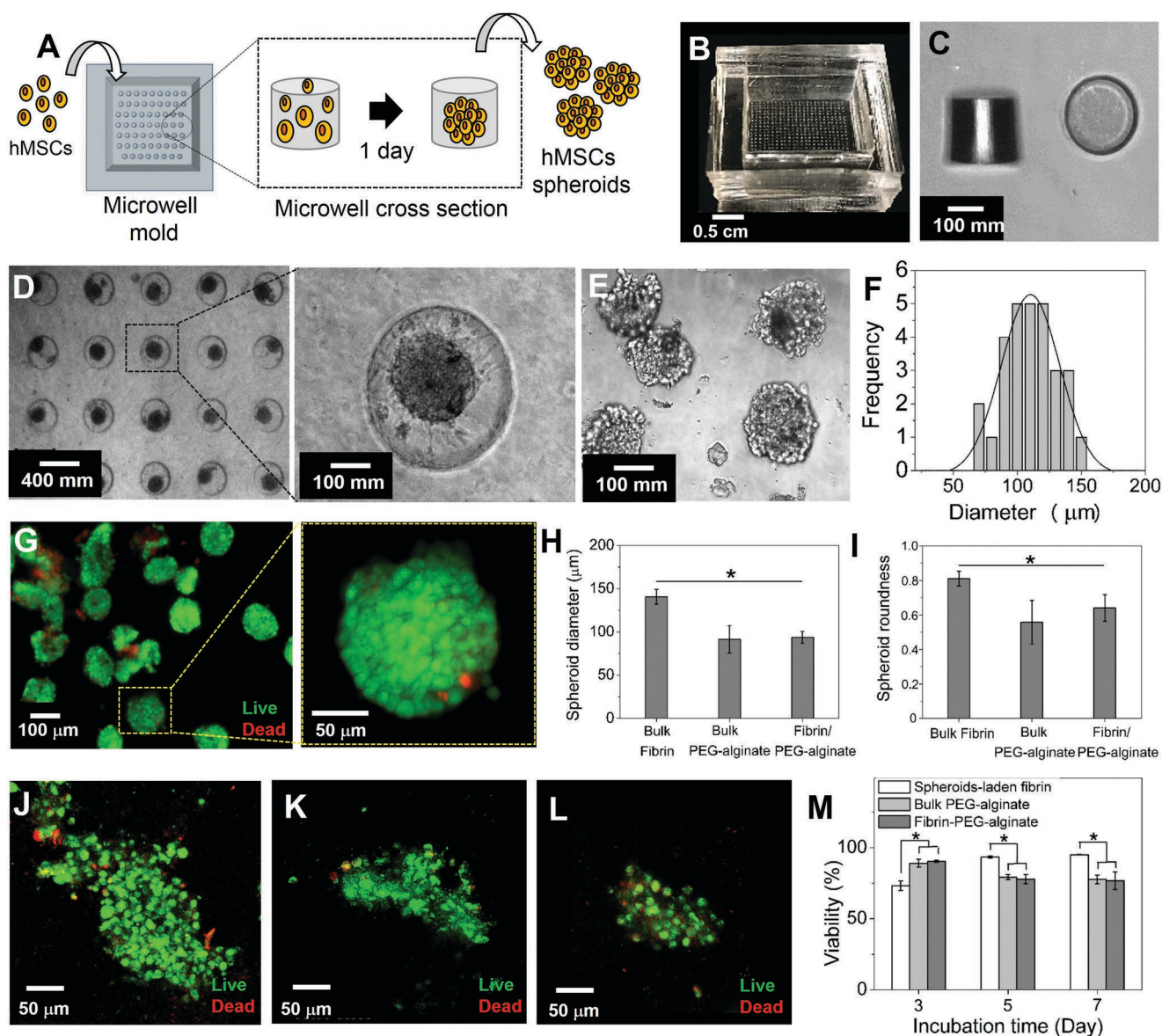
Figure 4. hMSC spheroid fabrication and characterization. A) Schematic of hMSC spheroid fabrication showing single cells being added to the microwell mold, forming spheroids after 1 d of culture. B) Picture of the PDMS mold. C) Optical image of a microwell mold. D) Optical image of hMSC spheroids in the PDMS mold after 1 day. E) Optical image of harvested spheroids after 1 d. F) Size distribution histogram of harvested spheroids. G) Confocal live/dead images of harvested spheroids. H) Diameter and I) roundness of spheroids in bulk fibrin, bulk 20% PEG–2.5% alginate and in fibrin/PEG–alginate, measured using ImageJ software. *$p < 0.05$. Confocal live/dead images of spheroids cultured in J) bulk fibrin, K) bulk 20% PEG–2.5% alginate and L) fibrin-laden in PEG–alginate for 7 d. M) Viability of spheroids cultured in bulk fibrin, bulk PEG–alginate hydrogel and fibrin/bulk gel (20% PEG–2.5% alginate hydrogel homogeneously mixed with fibrin) for 3, 5, and 7 d. *$p < 0.05$.

(Figure 5J), similar to the previously observed results for bovine serum albumin (BSA-FITC) (molecule with ≈3.3 nm of hydrodynamic radius) diffusion in fibrin gel.[23] Therefore, these findings demonstrate that bioprinting a soft hydrogel, e.g., fibrin (kPa) into a mechanically stiff hydrogel, e.g., PEG–alginate IPN can overcome common key limitations of mechanically strong hydrogels, e.g., poor diffusive capacities, by acting as diffusion highways for nutrients and cell signaling molecules (Figure 5K,L). Our approach thus represents a novel method to increase the survival and function of cells in stiff hydrogels (MPa).

We also assessed the chondrogenic activity of hMSC spheroids that were co-printed with fibrin gel in the PEG–alginate IPN hydrogel, and cultured in chondrogenic and regular media for 21 d. Chondrogenic-like differentiation was histologically visualized using Alcian blue for sulfated GAG's,[48] and Picrosirius red and Masson's trichrome for collagen.[49] In addition, immunohistochemical analysis of aggrecan deposition suggested a chondrogenic-like behavior of our system (Figure 5M). Semiquantitative image analysis confirmed that for all markers, ECM deposition was improved for the bioprinted spheroids cultured in chondrogenic medium as compared to constructs
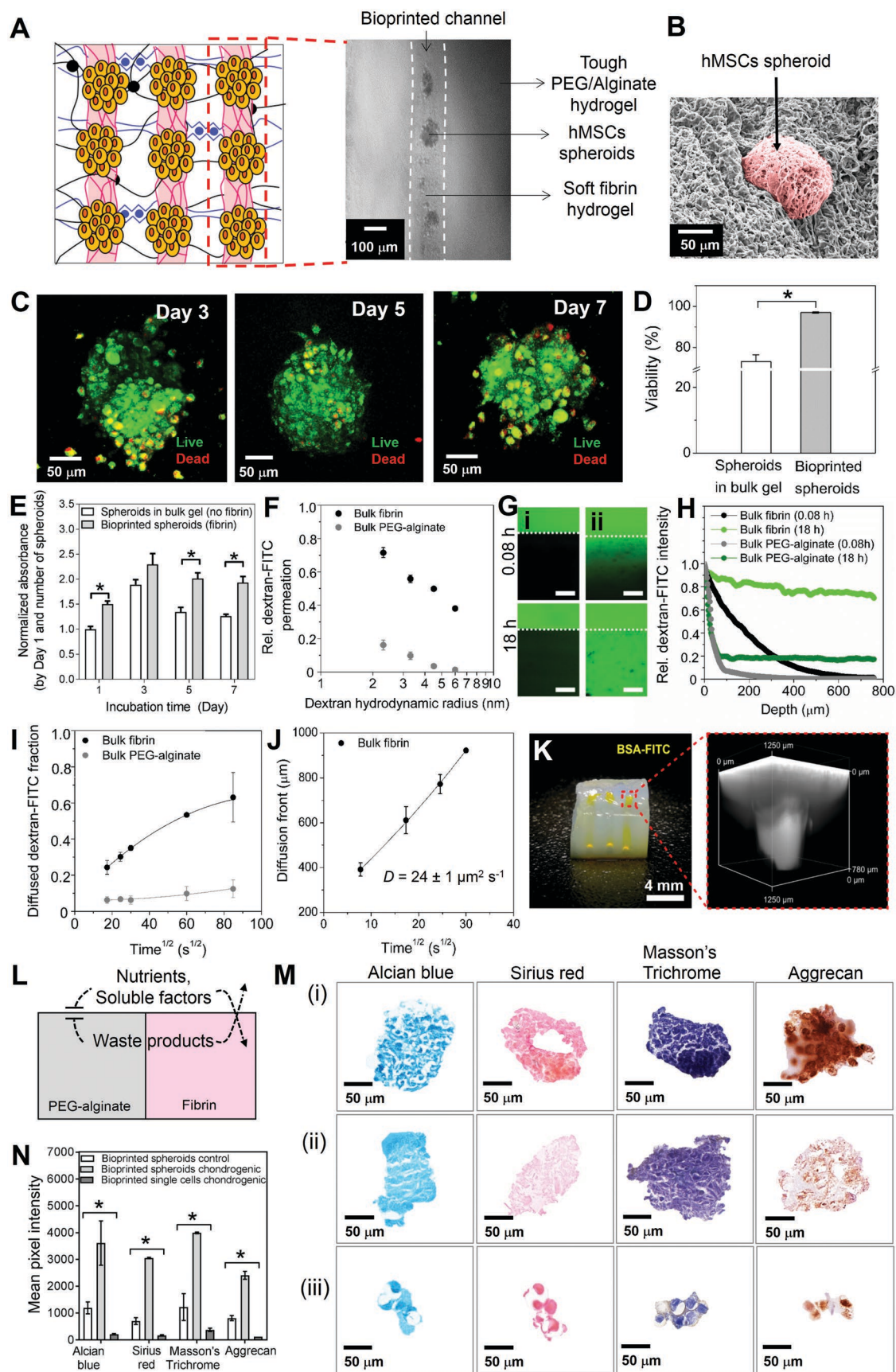
cultured in regular medium or as bioprinted single cells cultured that were exposed to chondrogenic media (Figure 5N). Indeed, microaggregating cells in micrometer sized spheroids is known to favor chondrogenic differentiation.[13,15]

Histological analysis revealed that hMSCs present in bioprinted spheroids that were induced to chondrogenic-like behavior showed a rounder morphology, while control cells presented greater eccentricity, or lengthening (Figure S7, Supporting Information), which is characteristic of nondifferentiated hMSCs.[50] These observations were in line with those reported in previous studies, reporting a higher capacity of hMSCs in spheroids to differentiate into chondrocytes in both in vitro and in vivo conditions, compared to single cells.[51,52]

This work showed that hMSC spheroids were successfully co-bioprinted with fibrin in a stiff and tough hydrogel, presenting high cell viability and a high capacity to differentiate into chondrocytes. Results indicated that the cartilage-like tissue engineering approach used here presents a great potential for further applications in cartilage regeneration studies.

3. Conclusion

We have developed a cartilage-like tissue by 3D bioprinting hMSC spheroid-laden fibrin in a stiff and tough biomaterial. It was demonstrated that dual crosslinking of PEG–alginate resulted in IPN hydrogels with mechanical properties in the MPa range, which is comparable to that of the native tissue, indicating the ability to withstand the mechanical loads that articular cartilage typically bears. In addition, IPN hydrogels showed a great capacity for resilience and elasticity, recovering their original shapes after up to 40% compressive cyclic loadings. A low viscosity bioink composed of fibrin was successfully printed in vertically oriented arrays within the PEG–alginate supporting bath in a macroscale crack-free manner, due to the shear-thinning behavior of the mixture. Fibrin gel showed high diffusive capacity, with a fast permeation rate of large molecules, indicating that bioprinted fibrin would facilitate nutrient diffusion throughout the stiff PEG–alginate IPN. The colloidal bioink composed of hMSC spheroids embedded in fibrin was readily extruded through the nozzle without damaging the cells, allowing the material to simulate the overall articular cartilage organization abstractly. Bioprinted hMSC spheroids showed significantly higher viability and metabolic activity after

7 d of culture as compared to spheroids in bulk PEG–alginate IPNs, demonstrating that the soft environment provided by fibrin and organized deposition contributed to cell survival. This environment favored chondrogenic-like differentiation, in which spheroids showed substantial GAG and collagen deposition after 3 weeks of culture. This innovative approach for cartilage-like tissue fabrication may be promising for further preclinical investigations of its utility for cartilage replacement and regeneration.

4. Experimental Section

Materials: Fibrinogen from bovine plasma, thrombin from bovine plasma, alginic acid sodium salt from brown algae (low viscosity, 100–300 cP), calcium chloride ($CaCl_2$), photoinitiator (2-hydroxy-4′-(2-hydroxyethoxy)-2-methylpropiophenone), proline, ascorbic acid, sodium pyruvate and dexamethasone were purchased from Sigma-Aldrich (St. Louis, MO, USA). Polyethylene glycol (PEG) dimethacrylate ($M_w = 1000$ Da) was purchased from Polysciences, Inc. (Warrington, PA, USA). Polydimethylsiloxane (PDMS) (Sylgard 184 Silicone Elastomer Kit) was purchased by Dow Corning (Midland, MI, EUA). Fluorescently labeled bovine serum albumin (BSA-FITC) and dextran molecules (Dextran-FITC) were purchased from Sigma Aldrich (St. Louis, MO, USA). Phosphate-buffered saline (PBS), fetal bovine serum (FBS), insulin-transferrin-selenium (ITS-Premix), penicillin–streptomycin (P/S), Dulbecco's modified eagle medium (DMEM), minimum essential media α (α-MEM), Live/dead viability/cytotoxicity Kit, PrestoBlue Kit and paraformaldehyde ampules were purchased from Thermo Fisher Scientific (Waltham, MA, USA). In Situ Cell Death Detection Kit, POD, was purchased from Roche Applied Sciences (Applied Biosystems, Foster City, CA). Basic fibroblast growth factor (FGF-b) and transforming growth factor β (TGF-β) were purchased from R&D Systems (Minneapolis, MN, EUA).

Fabrication of PDMS Molds: The negative for bioprinting the bath mold was fabricated by cutting (6 × 6 mm) a 6 mm thickness PMMA sheet using a laser cutting machine (VLS 2.30 Desktop Laser, Universal Laser Systems Inc, Richmond, VA), and the negative for the spheroids' mold consisted of 576 wells of 200 µm of height and diameter each, fabricated using standard soft photolithography technique. PDMS was prepared at a ratio of 10:1 of base to curing agent and poured into the negatives. After degassing in a vacuum chamber, the PDMS molds were cured at 80 °C for 1 h, cooled to room temperature, and demolded from their negative replicate.

Microscope Imaging: All bright field and fluorescent images were taken in a Nikon Eclipse Ti-S Microscope (Nikon, Tokyo, Japan) and all confocal images were taken in a ZEISS LSM 880 with Airyscan Microscope (Carl Zeiss, Jena, Germany). Scanning electron microscopy (SEM) images were taken on a LEO Electron Microscopy/Oxford (Cambridge, England).

Figure 5. Characterization of bioprinted hMSC spheroids in PEG–alginate hydrogel as a bioengineered cartilage construct. A) Bioprinted line showing a schematic illustration of the bioprinted spheroids in a tough hydrogel and a bright field image of the bioprinted line. B) Image captured by SEM of bioprinted spheroid-laden fibrin in a PEG–alginate hydrogel after 7 d, covered by fibrin hydrogel, which was false colored using ImageJ software. C) Live/dead images obtained by confocal of bioprinted spheroids on days 3, 5, and 7. D) Viability and E) Metabolic activity of spheroids in PEG–alginate and bioprinted spheroid-laden fibrin in 20% PEG–2.5% alginate. *$p < 0.05$. F) Relative permeation of dextran-FITC with a different hydrodynamic radius into the 10 mg mL^{-1} fibrin and 20% PEG–2.5% alginate hydrogels. G) Fluorescence confocal imaging of 20 kDa dextran-FITC diffusion through i) PEG–alginate and ii) fibrin hydrogels. Scale bars indicate 100 µm. H) Diffusion profiles of 20 kDa dextran-FITC into the hydrogels for 0.08 and 18 h. I) Diffusion of dextran-FITC into the hydrogels as function of time. J) Fickian diffusion of dextran-FITC (20 kDa) showing linear dependency with time and a diffusion coefficient, D, of 24 ± 1 µm^2 s^{-1}. K) BSA-FITC diffusion into a PEG–alginate hydrogel, with the image showing the increased permeation of BSA–FITC through the bioprinted fibrin lines as compared to the stiff IPN after 24 h. L) Schematic illustration of fibrin acting as a diffusion highway for nutrients and biomolecules to reach the spheroids, while PEG–alginate inhibits diffusion. M) Histological images of i) bioprinted spheroids cultured in chondrogenic medium, ii) regular medium (control) and iii) bioprinted single cells cultured in chondrogenic medium for 21 d and stained with Alcian blue for GAG's deposition, Picrosirius red and Masson's trichrome for collagen deposition, and immunohistochemical analysis for aggrecan deposition. N) Mean pixel intensity of stained bioprinted spheroids (in regular and chondrogenic mediums) and bioprinted single cells (in chondrogenic medium), measured using ImageJ software. *$p < 0.05$.

PEG–Alginate Hydrogels Fabrication: Dimethylacrylate PEG was dissolved in deionized (DI) water at concentrations of 30%, 40%, and 50%. Alginate solution in DI water (5%) was mixed with each PEG solution at a 1:1 ratio in order to prepare solutions with final concentrations of PEG 15%, 20%, and 25% with alginate 2.5%. After adding photoinitiator 0.25% and degassing, the mixture was carefully poured into the cubic PDMS mold, and placed in a UV chamber under UV light (365 nm wavelength) with a source of 200 mW cm^{-2} (Omnicure S2000, Excelitas Technologies, Salem, MA, USA) for 80 s. After the covalent PEG crosslinking, the hydrogel was removed from the mold and soaked in a 0.1 mol L^{-1} CaCl$_2$ solution for 1 h to ionically crosslink the alginate. After both PEG and alginate crosslinking, the hydrogels were taken to rheological and mechanical tests. For each condition, at least three samples ($n = 3$) were prepared.

Rheological and Mechanical Characterization: Rheological properties of prepolymers and hydrogels were analyzed using an Anton Paar MCR 702 TwinDrive rheometer (Anton Paar, Graz, Austria), operating with the top drive only. A 10 millimeter diameter parallel plate geometry was used for all measurements. For fibrinogen and PEG–alginate prepolymer solution, ≈1 mL of samples was used, and for crosslinked fibrin and PEG–alginate hydrogels, samples had ≈1 mm thickness; accordingly, the gap size was 1 mm in all cases. Temperature control was maintained using the P-PTD200 (bottom plate) and H-PTD200 (hood enclosure) attachments from Anton Paar, with cooling supplied by a Julabo circulating chiller. Results were recorded and analyzed using Anton Paar RheoCompass software. All measurements were performed at 25 °C. Prior to the measurement of each sample, the measuring system inertia (of the upper geometry) was calibrated to compensate for acceleration torque, and the motor was calibrated to compensate for residual friction. After these adjustments, the gap was recalibrated after which the samples were loaded and allowed to equilibrate for 30 min or until normal force had decayed. Mineral oil was added to the perimeter of the sample to prevent the sample from drying; frequency sweeps performed at the start and end of the measurements suggest that sample drying was not a significant issue. Mechanical tests were performed using a Zwick mechanical tester (Zwick/Roell, Ulm, Germany) with custom parallel plates. Compression measurements were recorded in the Test Xpert software by Zwick. All measurements were performed at room temperature. Samples were cut to have a circular cross section of 10.5 mm in diameter (L_0) and ≈1 mm in thickness. Prior to measurement, the zero gap was determined using the "approach" feature in the Test Xpert software. All measurements were performed at 1% L_0 s^{-1} (0.105 mm s^{-1}). For cyclic tests, after loading each sample, five cycles from 0% to 10% were performed sequentially; after the end of this test, the process was repeated to ensure that the results were reproducible up until 10% strain. Next, five cycles were performed from 0% to 20% strain. The final cycles were performed with increasing strain, starting at 0% strain and returning to 0% strain after each strain threshold: 10%, 20%, 30%, and 40%. Results from the final cycles, increasing strain cyclic tests at 10% and 20% were consistent with the individual trials at these strains. Compressive modulus was calculated as the slope of the stress–strain curve between 10% and 20% loading. The experiment was performed in triplicate ($n = 3$) for each condition.

Swelling Degree and Degradation Rate of IPN Hydrogels: PEG–alginate IPN hydrogels were dried under vacuum, and the dry weights (W_d) were measured. Afterward, samples were immersed in PBS for 72 h, and at predetermined time points, swollen hydrogels were weighed (W_s), and swelling degrees calculated by (%) = ($W_s − W_d$) /W_d × 100. Swollen hydrogels were dried and weighted (W_d) in order to obtain their degradation profile in PBS (control) and in sodium citrate 0.17 mol L^{-1}. Sodium citrate was used to accelerate alginate degradation, in a ratio of 0.77 (sodium citrate: alginate).[36] Results was expressed as mass loss (%) = ($W_i − W_d$)/W_i × 100. Both experiments were performed in triplicate ($n = 3$) for each condition.

Bioprinting Fibrin in PEG–Alginate Bath: In order to obtain fibrin as a bioink, fibrinogen was dissolved in saline solution (10 mg mL^{-1}) by gently mixing in a 37 °C water bath. PEG 20%–alginate 2.5% solution was used as the bath containing 0.25% photoinitiator and supplemented with 1 U per mL^{-1} thrombin to allow fibrin crosslinking during bioprinting. The bath was poured into the PDMS mold and left at 4 °C for at least 2 h. The bioprinting system consisted of two needles (diameter = 500 μm) glued to each other, with one needle connected to a 1 mm Teflon tube that in turn was connected to a 1 mL syringe containing the fibrinogen solution. The needle was placed in a syringe pump (New Era Pump Systems Inc., Suffolk County, NY) for bioink extrusion, with a controlled flow rate ranging from 5 to 10 μL min^{-1}. The bioprinting was performed using an INKREDIBLE 3D Bioprinter (Cellink, Gothenburg, Sweden) with the double needle connected to the print head, and the deposition was automatically controlled by a G-code. The nozzle speed ranged from 50 to 600 mm min^{-1}. Fibrin fibers were printed in at five different densities, 45, 75, 105, 135, and 165 lines cm^{-2}. At the end of the deposition step, the constructs were exposed to UV light (200 mW cm^{-2}) for 80 s and soaked in a 0.1 mol L^{-1} CaCl$_2$ solution for 30 min. To analyze the printed constructs, the fibrinogen was stained with pink dye during printing preparation, and images were taken using an optical microscope. The experiments were performed in triplicate ($n = 3$).

Diffusion Analysis: Fibrin and PEG–alginate hydrogels were combined with FITC-labeled BSA with a hydrodynamic radius of 3.3 nm (20 kDa), and dextran molecules with hydrodynamic radii of 2.3 nm (10 kDa), 3.3 nm, 4.5 nm (40 kDa), and 6.0 nm (70 kDa). The hydrogel constructs were then analyzed using fluorescence confocal imaging (Nikon A1+) and fluorescent intensity within and outside of the constructs was quantified using ImageJ software. The relative permeation of fluorescently labeled dextran molecules into hydrogels was determined by normalizing the fluorescent intensity within the hydrogels using the fluorescent intensity outside the hydrogels. Diffusion constant was determined by measuring the derivative of the diffusion front [μm] plotted against the square root of time [s$^{1/2}$], which is typically a linear plot in case of "Fickian" diffusion.

Cell Culture: Whole bone marrow was obtained from the posterior iliac crest of three adult donors under a protocol approved by the University Hospitals of Cleveland Institutional Review Board, and processed as previously described.[53] Isolation of hMSCs from the marrow was via a Percoll (Sigma) gradient and the differential cell adhesion method.[54] hMSCs were cultured in α-MEM, supplemented with 10% of FBS, 1% of P/S and 10 ng mL^{-1} of FGF-b. Culture media was refreshed every 2 d.

Spheroids Fabrication: The spheroids' PDMS mold was sterilized with ethanol 70%, changed at least four times every 30 min, and washed three times with PBS and two times with media. After trypsinization, hMSCs from passage 3 or 5 were seeded at a concentration of 1 × 10^6 cells in 200 μL media per mold, and allowed to settle in the wells for 1 h at 37 °C in a 5% CO$_2$ humidified incubator. Media was added to 1 mL and cells were kept in incubation until spheroids had formed. After 1 d, spheroids were carefully harvested via flow agitation and collected for culture and bioprinting. Spheroids were quantified in size distribution using ImageJ software.

Spheroids Culture in Fibrin Hydrogel: In order to evaluate their viability in fibrin, harvested spheroids fabricated with hMSCs from passage 5 were mixed in 160 μL of 10 mg mL^{-1} fibrinogen solution and added to a 48-well plate, followed by 36 μL of 0.1 U mL^{-1} thrombin and 4 μL of 0.1 mol L^{-1} CaCl$_2$ to allow for crosslinking. After gel formation, 700 μL of supplemented α-MEM was added to the wells and the plate was kept in incubation for 7 d, with 50% of the media changed every 2 d. To evaluate the spheroids' viability in a fibrin-hydrogel, spheroids were mixed in 50 μL of the fibrinogen solution, and added using a micropipette to the PDMS mold filled with PEG 20%–alginate 2.5% hydrogel containing 0.25% photoinitiator and supplemented with 1 U mL^{-1} thrombin to allow for fast fibrin crosslinking. PEG was crosslinked by UV light exposition (200 mW cm^{-2}) for 80 s, and alginate was crosslinked by soaking the hydrogel in a 0.1 mol L^{-1} CaCl$_2$ solution for 30 min. Hydrogels were placed in a 48-well plate containing 700 μL of supplemented α-MEM, and kept in incubation for 7 d, with 50% of the media changed every two days. Viability and metabolic activity of the spheroids were evaluated by using PrestoBlue reagent and live/dead kits. The experiment was performed in triplicate ($n = 3$) for each group.

Bioprinting Spheroids: Spheroids fabricated from hMSCs from passage 5 were mixed to the 10 mg mL^{-1} fibrinogen solution and added to a 1 mL syringe to be used as the bioink. Vertical constructs were bioprinted in a PEG 20%–alginate 2.5% hydrogel containing 0.25% photoinitiator and supplemented with 1 U mL^{-1} thrombin, using 200 mm min^{-1} as the flow rate and 6 µL min^{-1} as the extrusion speed. After bioprinting, the hydrogels were exposed to UV light (200 mW cm^{-2}) for 2 × 40 s, followed by soaking in 0.1 mol L^{-1} CaCl$_2$ for 30 min. The bioprinted constructs were placed in a 48- well plate filled with 700 µL of supplemented α-MEM, and kept in incubation for 7 d, with 50% of the media changed every two days until an assessment of viability. The experiment was performed in triplicate ($n = 3$).

Assessment of Spheroids Viability: PrestoBlue reagent was used to assess metabolic activity on days 3, 5, and 7. During each day, media was replaced by 10% of PrestoBlue reagent in α-MEM and spheroids were incubated for 3 h at 37 °C. An aliquot of 200 µL of the incubated reagent was transferred to a 96-well plate and absorbance read at 570 and 600 nm. The percentage of PrestoBlue reduction was calculated and results expressed as normalized absorbance (to the first day of culture and number of spheroids). Live/dead assay was carried out on days 3, 5, and 7 using live/dead kits. After washing the samples with PBS, samples were incubated for 30 min with an ethidium homodimer-1 and calcein mixture, previously prepared in a ratio of 3:1 in PBS. Then, samples were carefully washed with PBS and taken to a confocal microscope for imaging. Spheroids were visualized by Z-stacking 10 to 15 images, and the number of live and dead cells was calculated using ImageJ software. For each condition, three spheroids containing ≈1700 cells were counted. The experiment was performed in triplicate ($n = 3$) for each group.

Chondrogenic Differentiation: Bioprinted spheroids fabricated using hMSCs from passage 3 were cultured in chondrogenic medium DMEM, supplemented with 10% FBS, 1% P/S, 40 µg mL^{-1} proline, 50 µg mL^{-1} ITS-premix, 50 µg mL^{-1} ascorbic acid, 100 µg mL^{-1} sodium pyruvate, 10 mol L^{-1} dexamethasone and 10 ng mL^{-1} TGF-β1 for 21 d. Chondrogenic media was changed every third day. The experiment was performed in triplicate ($n = 3$).

Histological Preparations: Bioprinted constructs cultured in chondrogenic and control media were washed with PBS and fixed with 4% paraformaldehyde for 2 h. Afterward, the samples were rinsed twice with PBS, sliced (5 µm section) in paraffin blocks and kept in an oven at 65 °C for 2 h. The slices were deparaffinized in xylene and rehydrated in graded ethanol from 100% to 75%. Samples were stained with Alcian blue for GAG's, and Masson's trichrome and picrosirius red for collagen deposition. Slices were analyzed on cell death via a TUNEL assay using the In Situ Cell Death Detection Kit. Samples were scanned by digital slides scanner (3D Histech, MIDI). The experiment was performed in triplicate ($n = 3$).

Immunohistochemical Evaluation: Paraffin-embedded sections (5 µm) were deparaffinized in xylene, rehydrated in ethanol, and incubated with antiaggrecan rabbit pAb (1:500) overnight at 4 °C. Slices were washed with PBS (pH 7.4) and incubated with secondary antibody goat anti-rabbit IgG conjugated with HRP-polymer for 50 min at room temperature. Images were taken in a digital slides scanner (3D Histech, MIDI). The experiment was performed in triplicate ($n = 3$).

Statistical Analysis: All data are expressed as mean ± standard deviation. The nonparametric Kruskal-Wallis test was used to compared group means where $n = 3$ (Figures 2I, 3B,I,J, 4M, and 5D,E,N; Figure S1A,B, Supporting Information). One-way ANOVA with Tukey's test was used to compared groups where $n > 3$ that showed normative distribution (Figures 2C and 4H,I; Figure S7, Supporting Information). A p-value of 0.05 was considered significant.

Supporting Information

Supporting Information is available from the Wiley Online Library or from the author.

Conflict of Interest

The authors declare no conflict of interest.

[1] T. J. Klein, S. C. Rizzi, J. C. Reichert, N. Georgi, J. Malda, W. Schuurman, R. W. Crawford, D. W. Hutmacher, *Macromol. Biosci.* **2009**, *9*, 1049.

[2] J. Li, W. R. K. Illeperuma, Z. Suo, J. J. Vlassak, *ACS Macro Lett.* **2014**, *3*, 520.

[3] O. Jeon, J. Y. Shin, R. Marks, M. Hopkins, T. H. Kim, H. H. Park, E. Alsberg, *Chem. Mater.* **2017**, *29*, 8425.

[4] B. P. Partlow, C. W. Hanna, J. Rnjak-Kovacina, J. E. Moreau, M. B. Applegate, K. A. Burke, B. Marelli, A. N. Mitropoulos, F. G. Omenetto, D. L. Kaplan, *Adv. Funct. Mater.* **2014**, *24*, 4615.

[5] J. Y. Sun, X. Zhao, W. R. K. Illeperuma, O. Chaudhuri, K. H. Oh, D. J. Mooney, J. J. Vlassak, Z. Suo, *Nature* **2012**, *489*, 133.

[6] J. S. Park, J. S. Chu, A. D. Tsou, R. Diop, Z. Tang, A. Wang, S. Li, *Biomaterials* **2011**, *32*, 3921.

[7] O. Bas, E. M. De-Juan-Pardo, C. Meinert, D. D'Angella, J. G. Baldwin, L. J. Bray, R. M. Wellard, S. Kollmannsberger, E. Rank, C. Werner, T. J. Klein, I. Catelas, D. W. Hutmacher, *Biofabrication* **2017**, *9*, 025014.

[8] A. Buxboim, I. L. Ivanovska, D. E. Discher, *J. Cell Sci.* **2010**, *123*, 297.

[9] A. R. Gannon, T. Nagel, A. P. Bell, N. C. Avery, D. J. Kelly, *Eur. Cells Mater.* **2015**, *29*, 105.

[10] R. M. Schinagl, D. Gurskis, A. C. Chen, R. L. Sah, *J. Orthop. Res.* **1997**, *15*, 499.

[11] Q. Zhang, Y. Yu, H. Zhao, *Acta Biochim. Biophys. Sin.* **2016**, *48*, 958.

[12] Y. Fu, L. Karbaat, L. Wu, J. C. H. Leijten, S. Both, M. Karperien, *Tissue Eng., Part B* **2017**, *23*, 515.

[13] J. Leijten, L. S. Moreira Teixeira, J. Bolander, W. Ji, B. Vanspauwen, J. Lammertyn, J. Schrooten, F. P. Luyten, *Sci. Rep.* **2016**, *6*, 36011.

[14] R. A. Kosher, W. M. Kulyk, S. W. Gay, *J. Cell Biol.* **1986**, *102*, 1151.

[15] L. S. Moreira Teixeira, J. C. H. Leijten, J. Sobral, R. Jin, A. A. van Apeldoorn, J. Feijen, C. van Blitterswijk, P. J. Dijkstra, M. Karperien, *Eur. Cells Mater.* **2012**, *23*, 387.

[16] S. Hong, D. Sycks, H. F. A. Chan, S. Lin, G. P. Lopez, F. Guilak, K. W. Leong, X. Zhao, *Adv. Mater.* **2015**, *27*, 4034.

[17] H. Li, S. Liu, L. Lin, *Int. J. Bioprint.* **2016**, *2*, 10.

[18] G. O'Connell, J. Garcia, J. Amir, *ACS Biomater. Sci. Eng.* **2017**, *3*, 2657.

[19] T. Wang, J. H. Lai, F. Yang, *Tissue Eng., Part A* **2016**, *22*, 1348.

[20] K. Bootsma, M. M. Fitzgerald, B. Free, E. Dimbath, J. Conjerti, G. Reese, D. Konkolewicz, J. A. Berberich, J. L. Sparks, *J. Mech. Behav. Biomed. Mater.* **2017**, *70*, 84.

[21] J. Hendriks, C. Willem Visser, S. Henke, J. Leijten, D. B. F. Saris, C. Sun, D. Lohse, M. Karperien, *Sci. Rep.* **2015**, *5*, 11304.

[22] H. D. Guo, G. H. Cui, H. J. Wang, Y. Z. Tan, *Tissue Eng., Part A* **2011**, *17*, 45.

[23] A. Shkilnyy, P. Proulx, J. Sharp, M. Lepage, P. Vermette, *Colloids Surf., B* **2012**, *93*, 202.

[24] C. Perka, R. S. Spitzer, K. Lindenhayn, M. Sittinger, O. Schultz, *J. Biomed. Mater. Res.* **2000**, *49*, 305.

[25] C. Little, W. Kulyk, X. Chen, *J. Funct. Biomater.* **2014**, *5*, 197.

[26] J. S. Park, H. N. Yang, D. G. Woo, S. Y. Jeon, K. Park, *Biomaterials* **2011**, *32*, 1495.

[27] M. Sheykhhasan, R. T. Qomi, M. Ghiasi, *Int. J. Stem Cells* **2015**, *8*, 219.

[28] C. Colosi, S. R. Shin, V. Manoharan, S. Massa, M. Costantini, A. Barbetta, M. R. Dokmeci, M. Dentini, A. Khademhosseini, *Adv. Mater.* **2016**, *28*, 677.

[29] K. Zhu, S. R. Shin, T. van Kempen, Y. C. Li, V. Ponraj, A. Nasajpour, S. Mandla, N. Hu, X. Liu, J. Leijten, Y. D. Lin, M. A. Hussain, Y. S. Zhang, A. Tamayol, A. Khademhosseini, *Adv. Funct. Mater.* **2017**, *27*, 1605352.

[30] X. Cui, T. Boland, *Biomaterials* **2009**, *30*, 6221.

[31] G. R. Fulcher, D. W. L. Hukins, D. E. T. Shepherd, *BMC Musculoskeletal Disord.* **2009**, *10*, 61.

[32] J. Li, Z. Suo, J. J. Vlassak, *J. Mater. Chem. B* **2014**, *2*, 6708.

[33] M. Bartnikowski, R. M. Wellard, M. Woodruff, T. Klein, *Polymers* **2015**, *7*, 2650.

[34] Q. Chen, X. Yan, L. Zhu, H. Chen, B. Jiang, D. Wei, L. Huang, J. Yang, B. Liu, J. Zheng, *Chem. Mater.* **2016**, *28*, 5710.

[35] A. K. Bajpai, M. Shrivastava, *J. Appl. Polym. Sci.* **2002**, *85*, 1419.

[36] Z. Wu, X. Su, Y. Xu, B. Kong, W. Sun, S. Mi, *Sci. Rep.* **2016**, *6*, 24474.

[37] G. Hild, *Polymer.* **1997**, *38*, 3279.

[38] A. M. Grillet, N. B. Wyatt, L. M. Gloe, in *Rheology* (Ed: J. De Vicente), IntechOpen, London **2012**, pp 60–80.

[39] A. Akkaya, *J. Biol. Chem.* **2017**, *45*, 287.

[40] O. Moreno-Arotzena, J. G. Meier, C. Del Amo, J. M. García-Aznar, *Materials* **2015**, *8*, 1636.

[41] M. Huber, S. Trattnig, F. Lintner, *Invest. Radiol.* **2000**, *35*, 573.

[42] P. Chen, J. Mckittrick, M. A. Meyers, *Prog. Mater. Sci.* **2012**, *57*, 1492.

[43] N. S. Bhise, V. Manoharan, S. Massa, A. Tamayol, M. Ghaderi, M. Miscuglio, Q. Lang, Y. S. Zhang, S. R. Shin, G. Calzone, N. Annabi, T. D. Shupe, C. E. Bishop, A. Atala, M. R. Dokmeci, A. Khademhosseini, *Biofabrication* **2016**, *8*, 014101.

[44] B. Smeets, R. Alert, J. Pešek, I. Pagonabarraga, H. Ramon, R. Vincent, *Proc. Natl. Acad. Sci. USA* **2016**, *113*, 14621.

[45] K. C. Murphy, S. Y. Fang, J. K. Leach, *Cell Tissue Res.* **2014**, *357*, 91.

[46] Y. Sakai, K. Nakazawa, *Acta Biomater.* **2007**, *3*, 1033.

[47] B. H. Lee, M. H. Kim, J. H. Lee, D. Seliktar, N. J. Cho, L. P. Tan, *PLoS One* **2015**, *10*, e0118123.

[48] M. Adolphe, S. Thenet-Gauci, S. Demignot, in *In Vitro Methods in Pharmaceutical Research* (Eds: J. V. Castell, M. J. Gómez-Lechón), Academic Press, London **1996**, pp. 181–207.

[49] L. C. U. Junqueira, G. Bignolas, R. R. Brentani, *Histochem. J.* **1979**, *11*, 447.

[50] F. Haasters, W. C. Prall, D. Anz, C. Bourquin, C. Pautke, S. Endres, W. Mutschler, D. Docheva, M. Schieker, *J. Anat.* **2009**, *214*, 759.

[51] B. Johnstone, T. M. Hering, A. I. Caplan, V. M. Goldberg, J. U. Yoo, *Exp. Cell Res.* **1998**, *238*, 265.

[52] S. Suzuki, T. Muneta, K. Tsuji, S. Ichinose, H. Makino, A. Umezawa, I. Sekiya, *Arthritis Res. Ther.* **2012**, *14*, R136.

[53] S. E. Haynesworth, J. Goshima, V. M. Goldberg, A. I. Caplan, *Bone* **1992**, *13*, 81.

[54] O. Jeon, D. S. Alt, S. W. Linderman, E. Alsberg, *Adv. Mater.* **2013**, *25*, 6366.